Acquisition of cell migration defines NK cell differentiation from hematopoietic stem cell precursors

Barclay J. Lee[1,2] and Emily M. Mace[2,3]

[1]Department of Bioengineering, Rice University, Houston TX USA 77005

[2]Center for Human Immunobiology, Texas Children's Hospital, Houston TX USA 77030

[3]Department of Pediatrics, Baylor College of Medicine, Houston TX USA 77030

Corresponding author:

Emily Mace, PhD
Phone: 832-824-2217
Fax: 832-825-1260
mace@bcm.edu

Funding: This work was supported by the Virginia and L.E. Simmons Family Foundation and an American Society of Hematology Junior Faculty Scholar Award to EMM.

Abstract

Human natural killer (NK) cells are generated from $CD34^+$ precursors and can be differentiated *in vitro* by co-culture with developmentally supportive stromal cells. Despite the requirement for stromal cell contact in this process, the nature of these contacts has been poorly defined. We have previously identified a requirement for NK cell signaling receptors associated with terminal maturation in NK cell migration. However, the relationship between NK cell migration and differentiation, and how stromal cells drive NK cell maturation, is still unclear. Here, we perform continuous long-term imaging and tracking of NK cell progenitors undergoing *in vitro* differentiation. We demonstrate that NK cell precursors can be tracked over long time periods on the order of weeks by utilizing phase-contrast microscopy, and show that these cells acquire increasing motility as they mature. Additionally, we observe that NK cells display a more heterogeneous range of migratory behaviors at later stages of development. Overall, this work suggests an important interplay between NK cell development and motility and presents useful methods for additional research on this subject in long-term live-cell imaging workflows.

Introduction

Human natural killer (NK) cells are derived from $CD34^+$ hematopoietic stem cell precursors that are thought to originate in the bone marrow and undergo terminal maturation in secondary lymphoid tissue [1, 2]. Their differentiation has been stratified to 5 stages, with differential expression of surface markers, production of cytokines, and ability to perform cytotoxic functions [2, 3]. While originally these 5 stages were identified in secondary lymphoid and tonsillar tissue, it is now appreciated that NK cells can likely undergo maturation in a variety of microenvironments within the body [1, 4]. This has led to a model in which early NK cell precursors seed peripheral tissue and give rise to mature NK cells prior to entering circulation

Within peripheral blood, NK cells are found within the distinct functional and phenotypic subsets termed $CD56^{bright}$ or $CD56^{dim}$. $CD56^{dim}$ NK cells have strong cytolytic activity, expressing high levels of Fcγ receptor III (CD16), whereas $CD56^{bright}$ NK cells are $CD16^{+/-}$ with weaker natural cytotoxicity, but have greater production of immunoregulatory cytokines [5, 6]. The $CD56^{dim}$ subset seems to be more terminally differentiated than the $CD56^{brights}$, as higher cytokine production is associated with lesser maturation due to its requirement in the innate immune response to infection [1, 7]. Given, in part, the seeming plasticity in environments that can support NK cell development, as well as the poor correlation between human and murine NK cell phenotypes, human NK cell differentiation is a poorly understood process. In particular, understanding how NK cells interact with their microenvironment, and how this shapes the acquisition of function and phenotype, will enable a greater understanding of innate immune cell development and the contacts that promote it.

Human NK cell development can be studied with an *in vitro* model, which is also of interest for the generation of clinical grade NK cells for immune therapy [8, 9]. The most efficient method for *in vitro* differentiation of human NK cells from $CD34^+$ progenitor cells is through co-culture with an irradiated feeder layer of stromal cells, specifically the EL08.1D2 cell line [8, 10]. *In vitro* derived NK cells have cytotoxic function and exhibit many of the same surface markers observed on mature NK cells isolated derived from patient blood [1, 10-12]. NK cells can also be derived from progenitor cells in the presence of cytokines alone, but allowing contact with developmentally supportive stromal cells significantly increases cell proliferation as well as maturation [10, 11].

Despite the requirement for direct stromal cell contact in this system, the intercellular interactions between the $CD34^+$ progenitors and the EL08.1D2 cells driving this developmental pathway are as of yet unclear and deserve further study. Incubation of $CD56^{bright}$ or $CD56^{dim}$ NK cells on EL08.1D2 stroma leads to significant non-directed migration on stromal cells. Furthermore, isolation of NK cell developmental intermediates (NKDI) from tonsillar tissue or *in vitro* differentiation identifies distinct migratory behavior based upon developmental stage [13]. Stage 4 NK cells isolated from human tonsil tissue exhibit significantly faster cell migration and undergo less frequent arrests than less developed NKDI. Similarly, NKDI derived *in vitro* from $CD34^+$ stem cells exhibit progressively greater cell migration with time spent in culture. Additionally, disruption of CD56 function throughout development with a blocking antibody results in reduced migration velocities and a more constrained motility phenotype [13].

Lymphocytes generally have highly motile behaviors on a variety of substrates. Although exact speeds vary depending on experimental conditions, a typical T cell may migrate at roughly one body length per minute [14]. Migration is mediated by actin network remodeling within the cell, which is regulated by coordinated signals between integrins, including LFA-1 (CD11a/CD18, $\alpha L\beta 2$) and VLA-4 (CD49d/CD29, $\alpha 4\beta 1$) and the cytoskeleton [14]. Migrating lymphocytes are characterized by an active lamellipodia at the cell front and a uropod at the cell rear [14]. This polarized phenotype is demonstrated by migrating NK cells, which additionally undergo the formation of a developmental synapse between NK and stromal cells that is seemingly derived from a uropod structure [13]

Studies *in vivo* demonstrate the complexity of lymphocyte migration yet define classified behaviors. Lymphocyte migration heavily involves cell-cell interactions with the stromal environment, and two-photon microscopy shows that T cells crawl along stromal cells within the lymph node, emphasizing the role that the stromal network has on lymphocyte migration [15]. While NK cell migration *in vivo* is less well defined than that of T cells, intravital imaging of NK cells and $CD8^+$ T cells within tumors demonstrates that the two types of lymphocytes have distinct migration patterns [16]. In addition, NK cells may be directly activated through interactions with dendritic cells (DCs) expressing IL-15, despite relatively short periods of direct contact and reduced conjugate formation compared to T cells [17, 18].

With current microscopy technology it is now feasible to perform long-term time-lapse imaging of cells with sufficient time resolution to adequately track cell movements. Many modern microscope systems allow for temperature and environmental regulation

to ensure cell stability over a long period of time. Thus, a growing challenge in the field is how to best acquire and process large amounts of migration data in the most efficient and accurate manner. Typically, tracking is performed on cells labelled with a fluorescent dye such as CFSE, but this method is unsuited for long-term imaging, where phototoxicity and dye loss become problems [19]. Transmitted light microscopy avoids this issue, but makes tracking cells more difficult due to the lower signal-to-noise ratio in these images. In this case, tracking is often done manually, which is extremely time-consuming and allows for user bias. Reliable automated methods for tracking transmitted light images are thus highly desirable but currently lacking, although improvements have been made in recent years [20, 21].

In this study, we elucidate the mechanism behind *in vitro* NK cell differentiation from $CD34^+$ progenitor cells by studying how changes in cell motility relate to expression of known NK cell maturation markers. We show, for the first time, the continuous development of human NK cells from $CD34^+$ hematopoietic stem cells (HSCs) and demonstrate that the acquisition of motility is progressively acquired through NK cell maturation using unlabeled cells. We further quantify the heterogeneity in the developing NK cell migration phenotype by classifying single-cell tracks in terms of velocity and mode of migration (directed, constrained, or random). Together, this defines the acquisition of human NK cell migratory capacity throughout development using high temporal resolution and continuous length of imaging.

Methods

Cell culture

EL08.1D2 cells stromal cells were maintained on gelatinized culture flasks at 32° C in 40.5% α-MEM (Life Technologies), 50% Myelocult M5300 (STEMCELL Technologies), 7.5% heat-inactivated fetal calf serum (Atlanta Biologicals) with β-mercaptoethanol (10^{-5} M), Glutamax (Life Technologies, 2 mM), penicillin/streptomycin (Life Technologies, 100 U ml^{-1}), and hydrocortisone (Sigma, 10^{-6} M). Culture media was supplemented with 20% conditioned supernatant from previous EL08.1D2 cultures.

For *in vitro* $CD34^+$ differentiation, 96-well plates were treated with 0.1% gelatin in ultrapure water to promote cell adherence. Gelatinized 96-well plates were pre-coated with a confluent layer of EL08.1D2 cells at a density of 5-10 x 10^3 cells per well and then mitotically inactivated by irradiation at 300 rad. Purified $CD34^+$ hematopoietic stem cells were cultured at a density of 2-20 x 10^3 cells per well on these EL08.1D2 coated plates in Ham F12 media plus DMEM (1:2) with 20% human AB^- serum, ethanolamine (50 μM), ascorbic acid (20 mg l^{-1}), sodium selenite (5 μg l^{-1}), β-mercaptoethanol (24 μM) and penicillin/streptomycin (100 U ml^{-1}) in the presence of IL-15 (5 ng ml^{-1}), IL-3 (5 ng ml^{-1}), IL-7 (20 ng ml^{-1}), Stem Cell Factor (20 ng ml^{-1}), and Flt3L (10 ng ml^{-1}) (all cytokines from Peprotech). Half-media changes were performed every 7 days, excluding IL-3 after the first week.

NK92 cells were maintained in 90% Myelocult H5100 (STEMCELL Technologies) (Atlanta Biologicals) with IL-2 (200 U ml^{-1}). YTS cells were maintained in 85% RPMI 1640 (Life Technologies), 10% fetal calf serum (Atlanta Biologicals), HEPES (Life Technologies, 10 μM), penicillin/streptomycin (Life Technologies, 100 U ml^{-1}), MEM

Non-Essential Amino Acids Solution (Thermo Fisher, 1 mM), sodium pyruvate (1 mM), and L-glutamine (2 mM).

CD34$^+$ precursor isolation and flow cytometry

T and B cell lineage depletion was performed using NK cell RosetteSep (STEMCELL Technologies) and Ficoll-Paque density gradient centrifugation from routine red cell exchange apheresis performed at Texas Children's Hospital. Following pre-incubation with RosetteSep, apheresis product was layered on Ficoll-Paque for density centrifugation at 2,000 r.p.m. for 20 min (no brake). Cells were harvested from the interface and washed with PBS by centrifugation at 1,500 r.p.m. for 5 min then resuspended in fetal calf serum for cell sorting. All samples were obtained under guidance and approval of the Institutional Review Board of Baylor College of Medicine in accordance with the Declaration of Helsinki. T- and B- cell depleted cultures were incubated with antibodies for CD34 (clone 561, PE conjugate, BioLegend, 1:100) prior to sorting. FACS sorting was done using a BD Aria cell sorter with an 85 μm nozzle at 45 p.s.i. Purity after sorting was >90%. Primary NK cells for short-term imaging were isolated with NK cell RosetteSep.

For weekly FACS analysis of CD34$^+$ intermediates, a 6-colour flow cytometry panel was performed on a BD Fortessa using antibodies for CD56 (Clone HCD56, Brilliant Violet 605, BioLegend, 1:200), CD3 (Clone UCHT1, Brilliant Violet 711, BioLegend, 1:200), CD16 (Clone 3G8, PE-CF594 conjugate, BD, 1:300), CD94 (Clone DX22, APC conjugate, BioLegend, 1:100), CD117 (Clone 104D2, PE/Cy7 conjugate,

BioLegend, 1:10), and CD34 (clone 561, PE conjugate, BioLegend, 1:100). Flow cytometry data analysis was performed with FlowJo (TreeStar Inc.).

Live-cell imaging and tracking

Cells were imaged in 96-well ImageLock plates (Essen Bioscience) on the IncuCyte ZOOM Live-Cell Analysis System (Essen Bioscience) at 37° C every 5 minutes in the phase-contrast mode (10x objective). Images were acquired continuously for a 28-day period. NK cell lines and primary NK cells were labeled using CellTracker Violet (Thermo Fisher) for short-term imaging at a working concentration of 15 μM and washed with complete media by centrifugation at 1,500 r.p.m. for 5 minutes. Each cell type was seeded at 2 x 10^3 cells per well on a 96-well ImageLock plate that had been pre-seeded with EL08.1D2 cells, then imaged at 2 minute intervals for a 24-hour period. Images were exported to MATLAB for cell segmentation using custom scripts. Briefly, cell centroids were labeled by first applying a Gaussian filter to threshold image noise, then finding local minima on the filtered image. An edge filter was also applied to ignore minima corresponding to adherent stromal cells, which had less distinct edges in the phase-contrast images. An array of cell positions over time was generated and imported into Imaris (Bitplane) for tracking analysis. The image set was divided into 24 hour periods for tracking. Tracking was done using the Spot tracking method on Imaris with the 'Autoregressive Motion' setting and removing tracks below an automatic threshold on 'Track Duration'. Individual tracks were then verified by eye and corrected manually where necessary by using Imaris to fix broken or overlapping tracks.

Analysis

Track statistics were calculated using Imaris and exported as comma-separated value files which were graphed using GraphPad Prism. Mean speed was defined as the per-track average of all instantaneous speeds calculated at each frame. The straightness parameter was calculated by dividing the displacement by the total path length for each track, so that straightness values close to 1.0 represent highly directed tracks. Arrest coefficient was defined as the percentage of time that the cell stays in arrest based on a threshold on instantaneous speed of 2 μm/min, or approximately one cell body length per image interval. The standard deviation in velocity for each track was calculated as the standard deviation in instantaneous velocities observed. Rose plots were generated by selecting ~20 representative tracks per time series and plotting them in Imaris.

For mean squared displacement (MSD) analysis and classification of migration modes, we used custom MATLAB scripts based on a previously described method for transient migration behavior analysis [22]. Briefly, each track was analyzed using a sliding window approach and calculating the MSD corresponding to each window. The MSD data was fit to curve to estimate the degree of curvature and fit to a line to estimate the diffusion coefficient of the migration. Track segments were then classified as directed, constrained, or diffusive migration depending on thresholds on these values which were set to be the same as those previously described [22]. The threshold for diffusion coefficient was set at 4.2 $\mu m^2\ min^{-1}$, calculated based on the typical diameter of an NK cell, with all track segments having a smaller diffusion coefficient classified as constrained migration. On the other hand, all segments with an MSD curvature α above

1.5 were defined as directed migration. All remaining segments after these thresholds were applied were classified as diffusive migration.

Statistics

Statistical analysis was calculated using Prism 6.0 (GraphPad). Ordinary one-way ANOVA was used to compare track statistics. Statistical significance between MSD curves was evaluated by a Kruskal-Wallis test with Dunn's multiple comparison test. For all tests $P < 0.05$ was considered significant.

Results

Human NK cell types exhibit distinct migratory behavior on stromal cells

NK cell lines and *ex vivo* NK cells undergo migration on EL08.1D2 stromal cells when assayed over relatively short periods of imaging [13]. To compare their migratory behavior and validate the sensitivity of our long-term imaging system, we labeled NK92 and YTS cell lines, and *ex vivo* NK cells (eNK) with Cell Tracker Violet dye, and co-cultured them with EL08.1D2 cells for 24 hours. Cells were continuously imaged at 2 minute intervals, and following acquisition cells were tracked in Imaris using fluorescence mode (Fig. 1A). eNK and NK cell lines had distinct migratory properties in terms of their mean velocity, straightness, and arrest coefficient. Enriched NKs seemed to exhibit more directed motion overall, characterized by significantly higher track straightness and lower arrest coefficient (frequency of time of imaging found in arrest) than both cell lines (Fig. 1B, C). Interestingly, there were significant differences in motility between the two NK cell types, with NK92 cells having higher overall speeds than YTS cells (1.165±0.33 μm/min vs. 0.783±0.40 μm/min), although straightness was not significantly different (Fig. 1B, C). This is in agreement with previous reports of NK92 and YT cells (from which the YTS line is derived) showing differential migration within a Matrigel [23]. Collectively, these data demonstrate that the previously described migration of human eNK cells on stroma is recapitulated by NK cell lines, particularly the NK92 cell line.

Figure 1

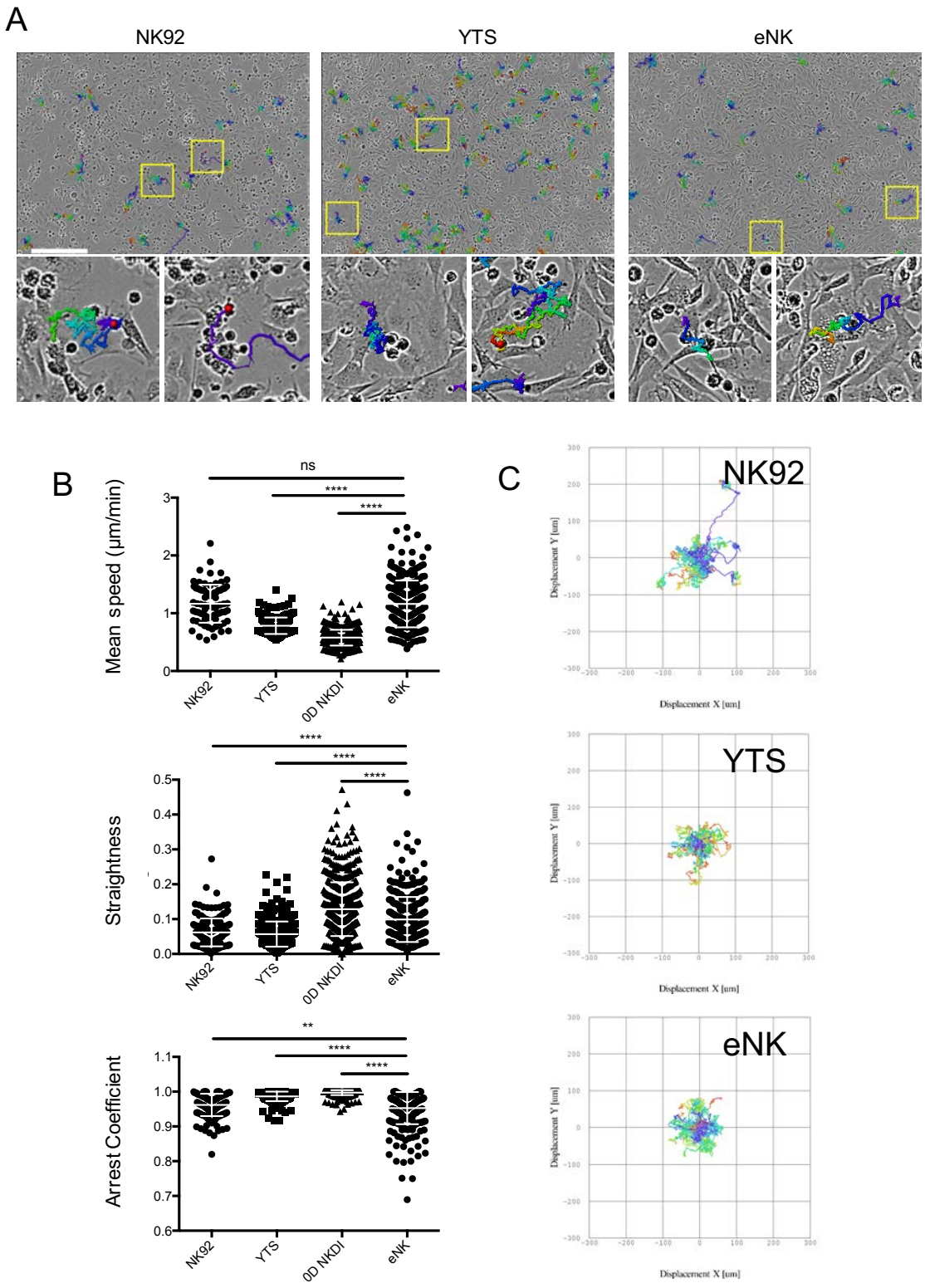

Figure 1. Continuous live cell imaging of human NK cells on stromal cells. YTS or NK92 NK cell lines or human NK cells (eNK) were co-cultured with an EL08.1D2 monolayer for 24 hours in a 96-well plate. Images were acquired continuously every 2 minutes and cells were tracked using a fluorescent label. A) Representative phase-contrast images of each cell type with randomly selected sample tracks overlaid. Insets show zoomed-in views of single-cell tracks. Scale bar=300 µm. B) Mean track speed (top), straightness (center), and arrest coefficient (bottom) of NK cells were calculated. Error bars indicate s.d. Means with significant differences were determined by ordinary one-way ANOVA with Tukey's multiple comparison test **p<0.01, ****p< 0.0001). Data is representative of three independent experiments. C) Rose plots of representative tracks.. n=30 per graph.

NK cell precursor motility and phenotype changes throughout maturation

As eNK cells show significant motility on stromal cells, and acquisition of migratory behavior is a feature of NK cell development *in vitro* and *in vivo* [13], we sought to define the migratory behavior of NK cell precursors throughout development. Using our long-term imaging system described above, we generated human NK cells *in vitro* from purified $CD34^+$ hematopoietic stem cells co-cultured on a developmentally supportive monolayer of EL08.1D2 stromal cells [10, 13]. Cells were imaged continuously every 5 minutes throughout the 28-day period required for maturation into NK cells (Fig. 2A). Individual cells were segmented and tracked for parameters including track speed, length and displacement to measure how their migratory behaviors evolved throughout differentiation (Fig. 2A, B). As expected, NK cell progenitors at the 0-day time point had significantly slower speeds than enriched NK cells (Fig. 1B). All tracking was done on phase-contrast images because we found that fluorescent cellular dyes did not persist throughout the entire four-week period (data not shown). Using this method enabled the tracking of single cells for extended periods of imaging (Fig. 2B, Supplemental Movie 1) and visual inspection confirmed that average cell track length increased significantly throughout the time of differentiation, even when stromal cells had undergone apoptosis and were no longer confluent (Fig. 2A, Supplemental Movies 2, 3).

To monitor the progression of NK cell development, we performed flow cytometry analysis of NK cell developmental markers at days 7, 14, 21, and 28. We analyzed cells for expression of CD117 and CD94, which, when considered with CD34, identify developmental stages 1-4, and CD16, a marker of NK cell terminal maturation [1, 3]. NK cells undergo differentiation through four linear stages: stage 1 cells are

Figure 2

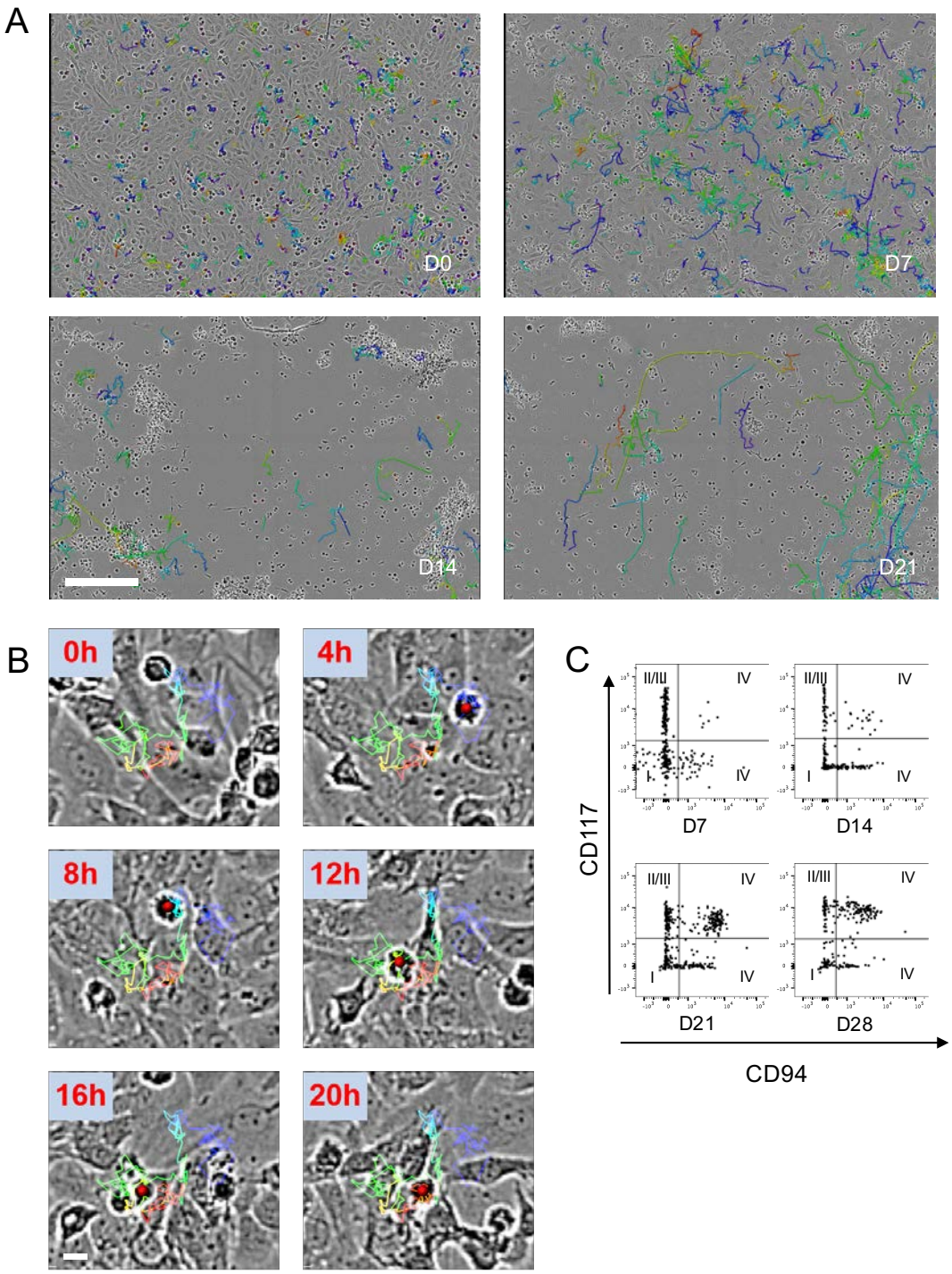

Figure 2. Acquisition of intrinsic NK cell migration with differentiation. CD34$^+$ HSCs were seeded on a monolayer of EL08.1D2 cells. Cells were imaged continuously in phase-contrast mode every 5 minutes for 28 days. FACS analysis was performed weekly to monitor expression of developmental markers. A) Representative images of NK cell intermediates with randomly selected tracks from one 24 hour imaging period overlaid. Scale bar=300 μm. B) Time coded track of a single NK precursor immediately after seeding onto EL08.1D2 monolayer. Scale bar=10 μm. C) FACS analysis of NK cell maturation markers. Predicted NK cell developmental stage based on phenotype as described in the text is shown in roman numerals.

$CD34^{+}CD117^{-}CD94^{-}$, stage 2/3 cells are $CD34^{+}CD117^{+}CD94^{-}$, and stage 4 cells are $CD34^{-}CD117^{+/-}CD94^{+}$. Increasing frequencies of cells underwent differentiation to stages 3 and 4 (35% at Day 28), which was accompanied by a decreasing frequency of immature cells at later time points (Fig. 2C). Therefore, changes in migratory behavior observed by imaging over the time of co-culture were accompanied by phenotypic profiles associated with NK cell differentiation.

NK cell precursors acquire increasing motility as they mature in vitro

To quantify the migratory behavior of developing NK cells, tracks were extracted from continuous 24 hour periods at days 0, 7, 14 and 21. Mean velocity, displacement, and track increased significantly at each progressive time point (Fig. 3A). Initially, $CD34^{+}$ cells had minimal velocity (0.58±0.14 μm/min), track length (255.58±131.07 μm), and displacement (31.91±21.54 μm). However, at day 21, mean velocity was 2.19±0.84 μm/min, consistent with previously reported migration speeds of mature NK cells [13, 22]. Similarly, track length and displacement from origin also underwent significant increases with progressive time points, particularly at days 14 and 21 (Fig. 3A). Given the significant differences between days 0 and 14, we performed tracking of consecutive 24-hour image sets over the first 14 days of imaging. Significant variations in mean speed, displacement, and path length were observed between daily time points, which cumulatively accounted for the overall trends previously described at the weekly time points (Fig. 3B). Therefore, the acquisition of track speed and length in developing NK cells occurs progressively throughout the initial stages of differentiation.

Figure 3

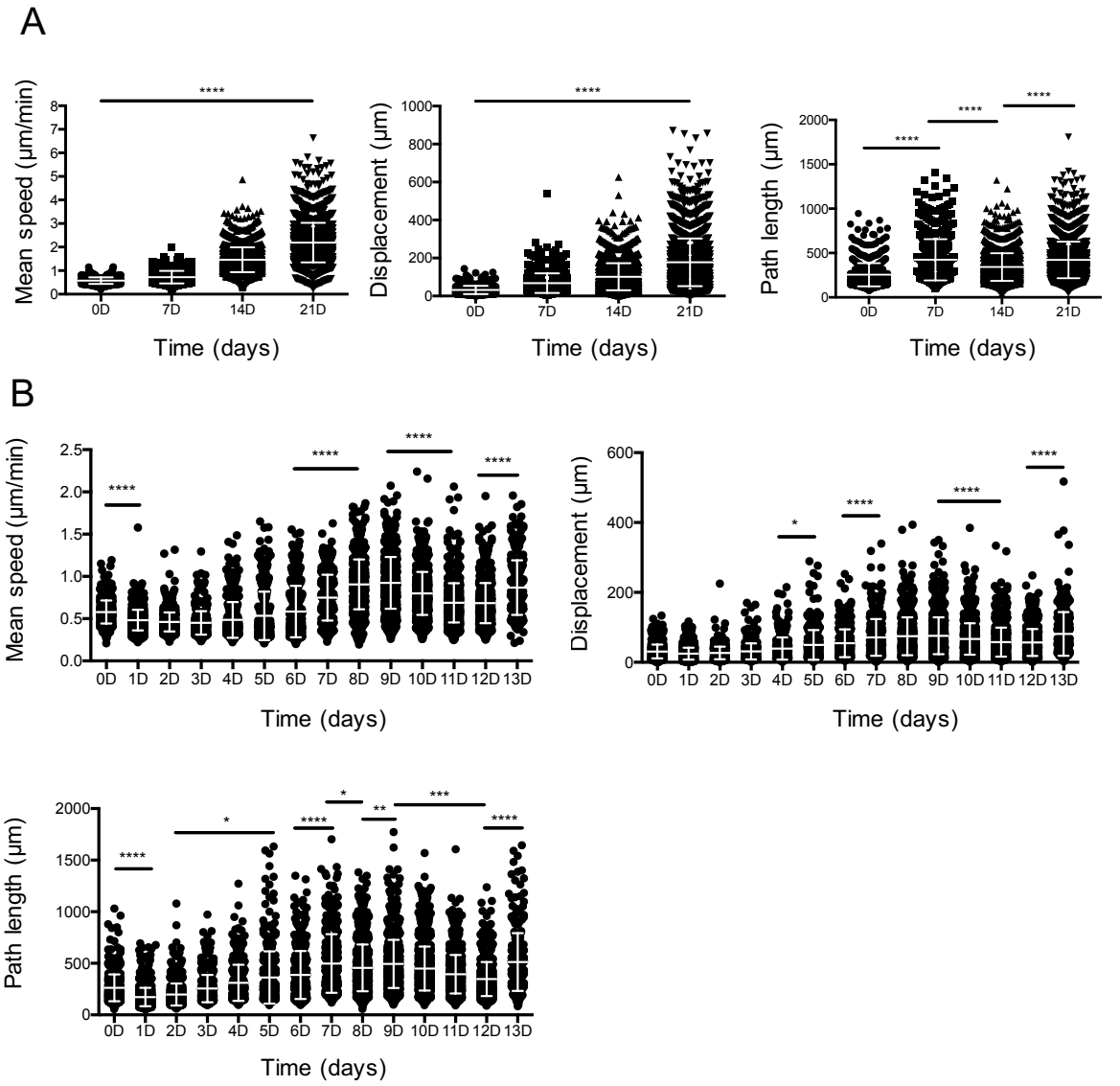

Figure 3. NK cell motility increases during cell development. A) Mean speed, displacement, and path length of NK cell developmental intermediates were imaged continuously for 28 days were measured at 7-day intervals as indicated. Error bars indicate s.d. ****p<0.0001 by ordinary one-way ANOVA with Tukey's multiple comparisons test. B) Mean speed, displacement, and path length of cells from continuous tracking from the first 14 days are shown as 24 hour segments. Error bars indicate s.d. Means with significant differences as analyzed by ordinary one-way ANOVA with Tukey's multiple comparison test are shown (*p< 0.05, **p<0.01, ***p<0.001, ****p<0.0001).

NK cell developmental intermediates in later stages of development exhibit more directed migration

Given the increasing speed and track length associated with migration of developing NK cells, we sought to further quantify the degree of directed migration in NK cell tracks by calculating the straightness and arrest coefficients. This was performed first on tracks extracted from 7-day intervals (Fig. 4A). An increase in straightness and decrease in arrest coefficient over time was observed for the weekly time points (Fig. 4A). While $CD34^+$ HSC (0D) had a track straightness of 0.13±0.08, at the 21D time point the mean straightness index was 0.42±0.20. Similarly, arrest coefficient decreased from 0.996±0.01 to 0.727±0.18 between the 0 and 21-day time points. This was in agreement with the increase in mean speed observed for the later time points. As demonstrated for the significant changes in track velocity between days 14 and 21, straightness and arrest coefficient similarly had the greatest changes in this time interval (Fig. 4A). Although significant differences from day to day were detected, the overall change in these statistics is relatively small compared to those observed in the last two weeks (Fig. 4B).

Mode of migration depends on NK cell developmental stage

Migrating cells can either exhibit directed motion, constrained motion, or random diffusion [24]. Random diffusion represents the type of movement expected of a cell of a certain size due to Brownian motion [22]. In this case, the mean square displacement (MSD) will be linear with time, whereas directed or constrained tracks will deviate above or below the linear trend, respectively [24]. To characterize the diffusivity of our NK cell

Figure 4

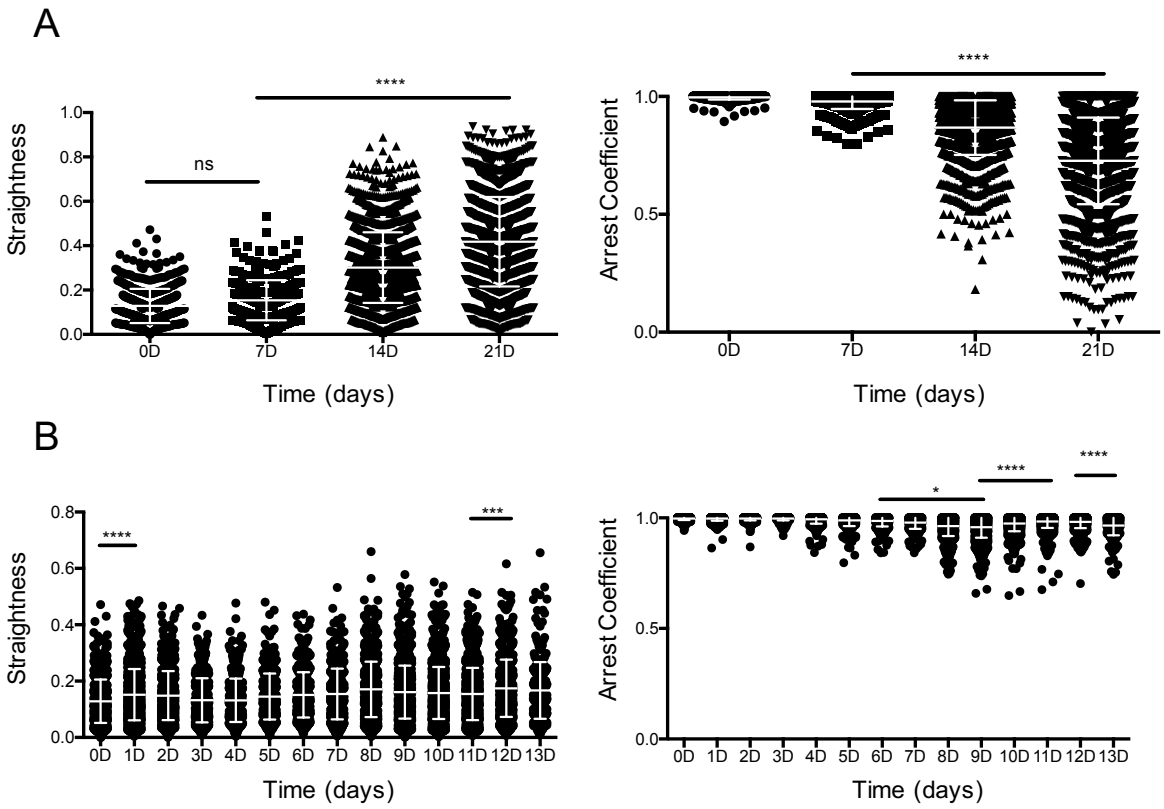

Figure 4. NK cell differentiation leads to increasingly directed migration. A) Straightness and arrest coefficient for NK cell tracks at weekly time points. Error bars indicate s.d. ****p<0.0001 by ordinary one-way ANOVA with Tukey's multiple comparison test. B) Straightness and arrest coefficient for NK cell tracks at daily time points. Error bars indicate s.d. Means with significant differences are determined by ordinary one-way ANOVA with Tukey's multiple comparison test (*p<0.05, ***p<0.001, ****p<0.0001).

precursors, we calculated the MSD of NK cell tracks at the weekly time points (Fig. 5A). In agreement with our previous measurements of track length and displacement, MSD progressively increased over time, starting at 1386.1±121.5 μm^2 at day 0 after t=450 minutes and increasing to 91483.0±20310.7 μm^2 at day 21 for the same t value.

While these values reflected a population-based measurement, many cells exhibited complex behaviors with multiple modes contained within a single track. To classify cell tracks by their transient properties, we implemented a previously described method for analyzing NK cell migration [22]. Using this method, for each track we calculated both the diffusion coefficient D and the diffusion exponent α, which define the slope and curvature of the MSD curve, respectively. Tracks were classified by mode of migration by thresholding on these values (Fig. 5B). Applying this analysis to all tracks for a given time point gave the fraction of time cells spent in either constrained versus directed migration. At day 0, the mean fraction of time cells exhibited constrained motion was 98% and the mean fraction of time cells underwent directed motion was only 0.5% (Fig. 5C). This had changed significantly by day 21, where the mean fraction for constrained motion decreased to 18.7% and the mean fraction for directed migration increased to 40.5% (Fig. 5D). These results suggest that the increase in mean speed over developmental stage that was described previously is due to a greater propensity for more mature cells to undergo directed migration.

Figure 5

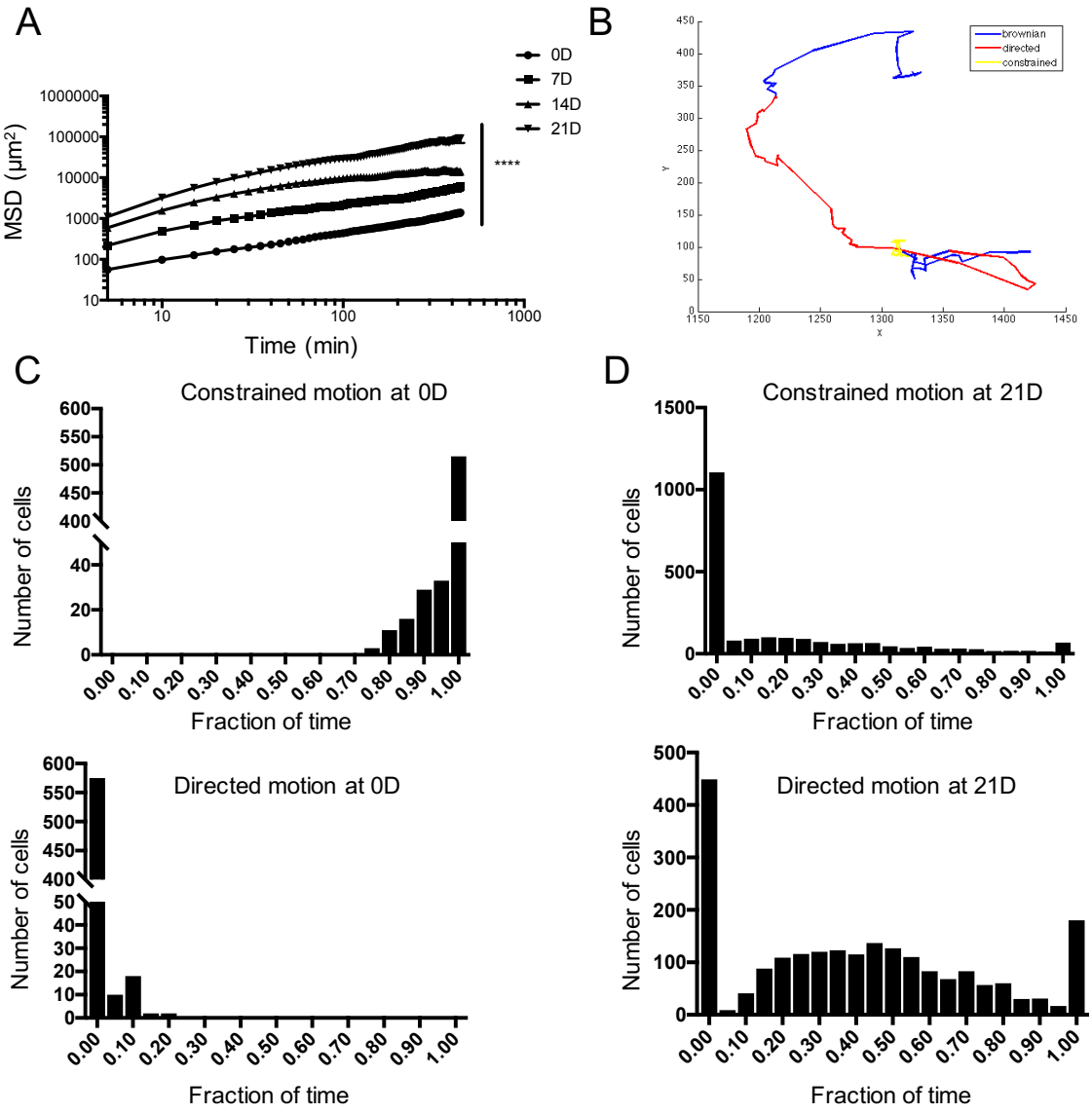

Figure 5. NK cell differentiation is associated with distinct modes of migration. A) Mean square displacement (MSD) of tracks acquired at weekly time points. Graph is truncated at roughly 450 min because few cell tracks persist for longer. Error bars indicate s.e.m. **** $p < 0.0001$ by Kruskal-Wallis test with Dunn's multiple comparison test. B) Representative NK cell track after 21 days of development shown with segments corresponding to each migration mode labeled. C) Fraction of time spent in either constrained or directed motion for each cell after 0 days of development. D) Fraction of time spent in either constrained or directed motion for each cell after 21 days of development.

NK cell maturation is accompanied by increased heterogeneity in NK cell migratory behavior

While we observed a global increase in cell motility over time, we also observed increasing heterogeneity of cell migratory behaviors with progressive NK cell maturation. Plotting the distribution of mean speeds for the 7-day time intervals, we observed that although mean speeds progressively increased over time, later time points still retained a few cells exhibited very low speeds (Fig. 6A). Individual analysis of single cell tracks shows that this increased variation in speed is accompanied by more diversity in migration behaviors (Fig. 6A). Increased standard deviation of track velocity at later time points was seen when we quantified both 24-hour and 7-day time intervals (Fig. 6B). Mean standard deviation increased from 0.32±0.12 μm/min at day 0 to 1.44±0.60 μm/min by day 21. At the beginning of tracking, cells exhibited primarily low-speed constrained tracks, whereas at later times there was a greater frequency of behavior such as Lévy-type super-diffusive walks, characterized by a series of short, constrained motions interspersed with periods of highly directed motion [24]. Additionally, a small subset of mature cells exhibited purely ballistic migration, travelling in essentially a straight line for the duration of migration, particularly at later time points (14 and 21 days).

Figure 6

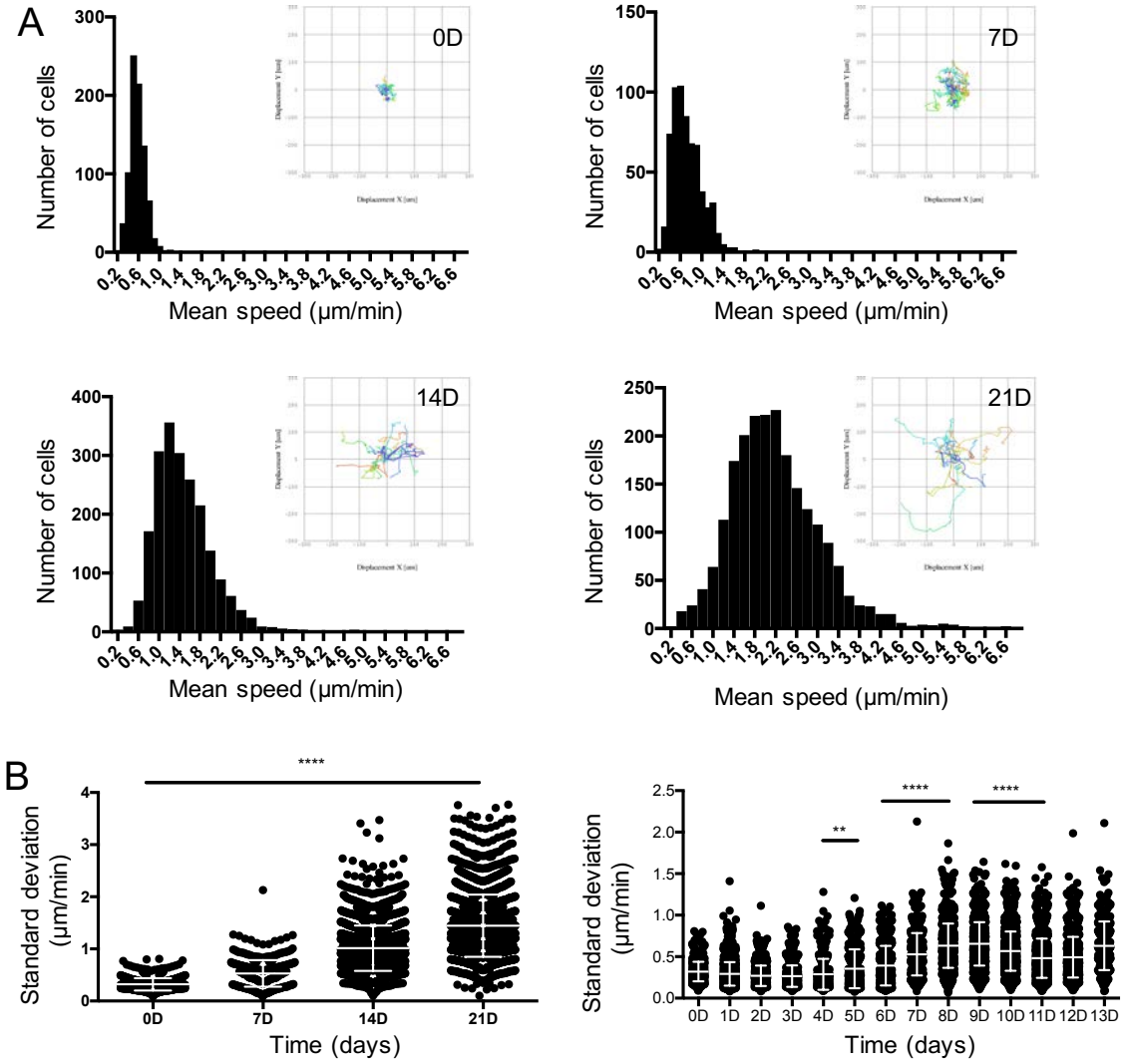

Figure 6. Cell maturation is correlated with increased heterogeneity of the migratory phenotype. A) Histogram of the mean speeds observed at the weekly time points. Insets: Rose plots of representative tracks. n=20 per graph. B) Standard deviation of the instantaneous speeds observed for each track for daily time points and weekly time points. Error bars represent s.d. Significance between means determined by ordinary one-way ANOVA with Tukey's multiple comparisons test (**p<0.01, ****p<0.0001)

Discussion

Lymphocyte motility is a critical behavior that enables their function, however the acquisition of migratory capacity through development, particularly by innate immune cells, is not well defined. Furthermore, there is intense interest in the use of *in vitro* generated human NK cells in the field of immune therapy, however the contribution of stromal cells utilized in these systems has not been defined. Therefore, understanding the nature of cell-cell contacts in human NK cell differentiation will lead to important biological and potentially therapeutic advances. By combining *in vitro* differentiation of human NK cells with highly temporally resolved, label-free imaging of developing NK cells, we have defined significant stages of NK cell motility that occur over the course of development, including changes in cell speed, mode of migration, and heterogeneity of migratory behaviors. Importantly, this progressive acquisition of motility occurs in NK cells derived entirely *in vitro*, thus defining migration as an NK cell intrinsic feature acquired through development.

Specifically, we observed that NK cell progenitors demonstrated significantly increased cell motility as they matured into functional NK cells. Continuous tracking of NKDI throughout development reveals that cells progressively acquire greater migratory capacity as well as more heterogeneous migration behaviors. A similar increase in velocity has been similarly described in developing human T cells, as relatively immature (double-negative and double-positive) thymocytes have substantially slower track speeds than their more mature single-positive counterparts [25, 26]. It seems clear that increased migration is acquired throughout lymphocyte development as a means for enhancing cytolytic effectiveness. On average, observed progenitor cell velocities at

all stages were similar to typical velocities seen for immortalized NK cell lines as well as those seen in other studies looking at lymphocyte motility, both *in vitro* [22, 27] and *in vivo* [26, 28].

By analyzing the mean squared displacement of cell tracks, we observed significantly more directed walks at later stages of NK cell differentiation. This could reflect a migration strategy adopted by more functional NK cell intermediates to maximize target cell killing. Many cells measured at later time points exhibited Lévy-type walks, characterized by periods of extended cell arrest interspersed with short, highly directional movements. $CD8^+$ T cells similarly utilize Lévy walks, with computational modeling suggesting that this behavior increases the efficiency of locating target cells compared to a purely random walk [29]. Inhibiting T cell turning, such as through deletion of the non-muscle myosin motor myosin 1g, leads to decreased detection of rare antigens and supports the idea that an inability to effectively perform Lévy-type walks results in a less efficient search strategy [30]. In NK cells, similar transient periods of arrest have been previously described to correspond to the formation of conjugates with target cells and cell-mediated killing, although they can also occur spontaneously [22]. Interestingly, IL-2-activated NK cells, which have greater cytolytic activity than unstimulated cells, spend much less time in arrest while also forming twice as many cell contact compared to resting NK cells, suggesting that regulation of this behavior correlates with relevant functional differences [31]. Therefore, the acquisition of this specific mode of migration may represent a previously unappreciated component of functional maturation. Alternatively, the seeking behavior that develops may enable the location of key developmental cues that are required for NKDI to proceed through

differentiation. It will be of interest to determine whether this behavior is a requirement for, or a product of, NK cell maturation.

At least initially, migration of NK cell developmental intermediates involves interactions between NK cell progenitors and EL08.1D2 stromal cells. NK cell intermediates may initially preferentially adhere to viable stromal cells through integrin ligands or other cell adhesion molecules, causing a bias towards more constrained migration. However, after 10-14 days of *in vitro* culture, many of the stromal cells underwent apoptosis, possibly due to NKDI-mediated cytotoxicity. This loss of confluent stromal cells may lead to the increased frequency of directed walks we measured as there are fewer stromal cells to provide a constraining effect. Surprisingly, we observed that NKDI continued to exhibit transient periods of arrest at the later time points when almost no stromal cells remained adherent to the plate.

Intravital microscopy demonstrates that lymphocytes closely interact with the stromal microanatomy in lymph nodes and form frequent cell-cell contacts, suggesting that direct interactions with stroma drives NK cell migration [15, 17, 28]. NK cells also interact with EL08.1D2 stromal cells through a uropod-derived structure termed the developmental synapse, at which CD56 and CD62L are enriched [13]. While EL08.1D2 stromal cells are derived from murine fetal liver, they express conserved extracellular matrix components including NCAM and fibronectin [13]. Given the requirement for EL08.1D2 stroma in the efficient generation of mature NK cells in this system, yet the cross-species nature of these interactions, it is likely that conserved molecules such as ECM components are a key contribution of this cell line to the generation of mature NK cells. As NKDI continue to migrate and exhibit significant adhesion even following loss

of EL08.1D2 confluence, it is further likely that the secretion of ECM components by the stromal cell line continues to act as a platform for NKDI migration and development. Alternatively, developmentally supportive stromal cells may secrete chemokines that contribute, at least initially, to NK cell migration. Hematopoietic progenitor cells express chemokine receptors such as CCR7 and CXCR4 and migrate in response to ligands against these receptors [32, 33]. Lymph node stromal cells express chemokines such as CXCL13 [15] as well as other motility-promoting factors such as autotaxin [34]. Recently, it was also found that bystander cells can enhance NK cell killing of target cells by producing H_2O_2, which provides a local acceleration of NK cell motility around bystanders [27]. Given the requirement for direct stromal cell contact with progenitors for the generation of mature NK cells, however, it is likely that at least part of the stromal cell contribution to NK cell development is a supportive substrate.

Finally, while we have studied NK cell migration in a two-dimensional system, lymphocyte migration in 2D and 3D environments may be differentially regulated [27, 30, 35]. It will be of interest to extend these findings to a three-dimensional environment through the use of Matrigel or microchannel-based platforms [23, 36]. Understanding the more complex interactions within a developmentally supportive microenvironment will provide even greater insight into the nature of contacts that drive human NK cell maturation.

In summary, we have shown that NK cells acquire motility throughout development, transitioning from a mostly constrained migratory phenotype to exhibiting Lévy-type walks and more directed migration. The transition to this mode of migration strategy may enable more efficient target cell killing by increasing the rate at which NK

cells can conjugate with targets. Additionally, the increased heterogeneity in cell migration at later stages may correspond to NK cells with different functional capabilities, with cells exhibiting greater motility being more effective at cell-mediated cytotoxicity. Continuing to study NK cell dynamics at the single-cell level will likely lead to greater understanding of their development and function.

Acknowledgments

We thank Dr. Alexandre Carisey for assistance with coding and useful scientific discussion, and Dr. Michael Diehl for critical reading of the manuscript. EL08.1D2 stromal cells were a kind gift from Drs. Jeffrey Miller and Elaine Dzierzak.

Supplemental movie legends

Supplementary Movie 1. Zoomed-in video of a single-cell track 0 days after the culture was set up. Visualizes the time series shown in Fig. 2C.

Supplementary Movie 2. Live-cell microscopy imaging of the co-culture 0 days after initiation of tracking. Randomly selected cell tracks are overlaid.

Supplementary Movie 3. Live-cell microscopy imaging of the co-culture 7 days after initiation of tracking. Randomly selected cell tracks are overlaid.

References

1. Eissens, D.N., et al., *Defining early human NK cell developmental stages in primary and secondary lymphoid tissues.* PLoS One, 2012. **7**(2): p. e30930.
2. Freud, A.G., et al., *A human CD34(+) subset resides in lymph nodes and differentiates into CD56bright natural killer cells.* Immunity, 2005. **22**(3): p. 295-304.
3. Freud, A.G., et al., *Evidence for discrete stages of human natural killer cell differentiation in vivo.* J Exp Med, 2006. **203**(4): p. 1033-43.
4. Yu, J., A.G. Freud, and M.A. Caligiuri, *Location and cellular stages of natural killer cell development.* Trends Immunol, 2013. **34**(12): p. 573-82.
5. Cooper, M.A., et al., *Human natural killer cells: a unique innate immunoregulatory role for the CD56bright subset.* Blood, 2001. **97**(10): p. 3146.
6. Nagler, A., et al., *Comparative studies of human FcRIII-positive and negative natural killer cells.* The Journal of Immunology, 1989. **143**(10): p. 3183.
7. Bancroft, G.J., *The role of natural killer cells in innate resistance to infection.* Curr Opin Immunol., 1993. **5**(4): p. 503-10.
8. Dezell, S.A., et al., *Natural killer cell differentiation from hematopoietic stem cells: a comparative analysis of heparin- and stromal cell-supported methods.* Biol Blood Marrow Transplant, 2012. **18**(4): p. 536-45.
9. Rezvani, K. and R.H. Rouce, *The Application of Natural Killer Cell Immunotherapy for the Treatment of Cancer.* Frontiers in Immunology, 2015. **6**(578).
10. Grzywacz, B., et al., *Coordinated acquisition of inhibitory and activating receptors and functional properties by developing human natural killer cells.* Blood, 2006. **108**: p. 3824-3833.
11. Miller, J.S. and V. McCullar, *Human natural killer cells with polyclonal lectin and immunoglobulinlike receptors develop from single hematopoietic stem cells with preferential expression of NKG2A and KIR2DL2/L3/S2.* Blood, 2001. **98**(3): p. 705.
12. Sivori, S., et al., *Early expression of triggering receptors and regulatory role of 2B4 in human natural killer cell precursors undergoing in vitro differentiation.* PNAS, 2002. **99**(7): p. 4526-31.
13. Mace, E.M., et al., *Human NK cell development requires CD56-mediated motility and formation of the developmental synapse.* Nat Commun, 2016. **7**: p. 12171.
14. Dupré, L., et al., *T Lymphocyte Migration: An Action Movie Starring the Actin and Associated Actors.* Frontiers in Immunology, 2015. **18**.
15. Bajénoff, M., et al., *Stromal Cell Networks Regulate Lymphocyte Entry, Migration, and Territoriality in Lymph Nodes.* Immunity, 2006. **25**(6): p. 989-1001.
16. Deguine, J., et al., *Intravital imaging reveals distinct dynamics for natural killer and CD8(+) T cells during tumor regression.* Immunity, 2010. **33**(4): p. 632-44.
17. Beuneu, H., et al., *Dynamic behavior of NK cells during activation in lymph nodes.* Blood, 2009. **114**(15): p. 3227-34.
18. Deguine, J. and P. Bousso, *Dynamics of NK cell interactions in vivo.* Immunol Rev, 2013. **251**(1): p. 154-9.

19. Coutu, D.L. and T. Schroeder, *Probing cellular processes by long-term live imaging--historic problems and current solutions.* J Cell Sci, 2013. **126**(Pt 17): p. 3805-15.
20. Hilsenbeck, O., et al., *Software tools for single-cell tracking and quantification of cellular and molecular properties.* Nat Biotechnol, 2016. **34**(7): p. 703-6.
21. Xing, F. and L. Yang, *Robust Nucleus/Cell Detection and Segmentation in Digital Pathology and Microscopy Images: A Comprehensive Review.* IEEE Rev Biomed Eng, 2016. **9**: p. 234-63.
22. Khorshidi, M.A., et al., *Analysis of transient migration behavior of natural killer cells imaged in situ and in vitro.* Integr Biol (Camb), 2011. **3**(7): p. 770-8.
23. Edsparr, K., et al., *Human NK cell lines migrate differentially in vitro related to matrix interaction and MMP expression.* Immunol Cell Biol, 2009. **87**(6): p. 489-95.
24. Krummel, M.F., F. Bartumeus, and A. Gerard, *T cell migration, search strategies and mechanisms.* Nat Rev Immunol, 2016. **16**(3): p. 193-201.
25. Halkias, J., et al., *Opposing chemokine gradients control human thymocyte migration in situ.* J Clin Invest, 2013. **123**(5): p. 2131-42.
26. Ehrlich, L.I., et al., *Differential contribution of chemotaxis and substrate restriction to segregation of immature and mature thymocytes.* Immunity, 2009. **31**(6): p. 986-98.
27. Zhou, X., et al., *Bystander cells enhance NK cytotoxic efficiency by reducing search time.* Sci Rep, 2017. **7**: p. 44357.
28. Miller, M.J., et al., *Two-Photon Imaging of Lymphocyte Motility and Antigen Response in Intact Lymph Node.* Science, 2002. **296**: p. 1869-1873.
29. Harris, T.H., et al., *Generalized Levy walks and the role of chemokines in migration of effector CD8+ T cells.* Nature, 2012. **486**(7404): p. 545-8.
30. Gerard, A., et al., *Detection of rare antigen-presenting cells through T cell-intrinsic meandering motility, mediated by Myo1g.* Cell, 2014. **158**(3): p. 492-505.
31. Olofsson, P.E., et al., *Distinct Migration and Contact Dynamics of Resting and IL-2-Activated Human Natural Killer Cells.* Front Immunol, 2014. **5**: p. 80.
32. Kim, C.H. and H.E. Broxmeyer, *SLC/exodus2/6Ckine/TCA4 induces chemotaxis of hematopoietic progenitor cells: differential activity of ligands of CCR7, CXCR3, or CXCR4 in chemotaxis vs. suppression of progenitor proliferation.* J Leukoc Biol., 1999. **66**(3): p. 455-61.
33. Aiuti, A., et al., *The chemokine SDF-1 is a chemoattractant for human CD34+ hematopoietic progenitor cells and provides a new mechanism to explain the mobilization of CD34+ progenitors to peripheral blood.* J Exp Med, 1997. **185**(1): p. 111-20.
34. Katakai, T., et al., *Autotaxin produced by stromal cells promotes LFA-1-independent and Rho-dependent interstitial T cell motility in the lymph node paracortex.* J Immunol, 2014. **193**(2): p. 617-26.
35. Wu, P.-H., et al., *Three-dimensional cell migration does not follow a random walk.* Proceedings of the National Academy of Sciences, 2014. **111**(11): p. 3949-3954.

36. Jacobelli, J., et al., *Confinement-optimized three-dimensional T cell amoeboid motility is modulated via myosin IIA-regulated adhesions.* Nat Immunol, 2010. **11**(10): p. 953-61.